Sreyas International Journal of Scientists and Technocrats, Vol. 1(1) 2016, pp. 28-32

RESEARCH ARTICLE

Modeling of Phase Changes of Hypo Eutectoid Steels

[*]Suresh Akella[1], B Ramesh Kumar[2]
[1]Sreyas Institute of Engineering & Technology, Nagole, Hyderabad 500068, India.
[2]Institute of Plasma Research, Bhat, Gandhinagar- 382428, India.

Received- 15 October 2016, Revised- 30 November 2016, Accepted- 20 December 2016, Published- 30 December 2016

ABSTRACT

Austenitic steels have low carbon content and belong to the hypo eutectoid range such as SS304, SS304L and SS316. These steels are preferred material for nuclear welded structures. The computational modeling of the welding process is required to compute the distortion and residual stresses. This work is about the phase changes and incorporation of the alloy elements in the Iron – iron carbide diagram.

Keywords: Austenitic steels, Hypo eutectoid, Distortion stress, Residual stress, Iron -Iron carbide.

1. INTRODUCTION

Austenitic stainless steels are the most used stainless steels, with normal yield strength of 210MPa, like mild steel and are corrosion resistant in most environments [1]. Since carbon content is below eutectoid point, this falls in hypo eutectoid range. Welding simulation is a coupled thermo - metallurgical - structural simulations. A model is needed for microstructure evolution which can be the discretization model that is based on density. However, solid state transformation for fully stabilized steel includes carbon diffusion, precipitate size and grain growth. There are different models [2-4] based on works by Leblond, Johnson-Mehl, Avrami etc. In this study, the Kirkaldy model used by Goldak, Akhlagi, Lingren and others is used [5, 6].

American Iron and Steel Institute (AISI) defined 200 series with higher carbon content in where the popular 300 series is widely used that is mainly preferred for corrosion resistance. 304 along with 304L series is mostly used in 300 series. In 316 series, 2% Cr replaces equivalent % of Mo in order to enhance pitting corrosion. L, low carbon grades became popular with the advent of low cost melting process, Argon Oxygen Decarburization (AOD). Austenitic steels are hypo eutectoid steels with carbon content less than eutectoid composition of 0.76%. The lever rule determines the percentage of cementite.

In welding of stainless steels, Lindgren from the computations and experiments concluded that thermal properties, heat conduction, heat capacity and latent heat are more dominant in distortion during welding than the mechanical properties of elasticity and plasticity. [7, 8] Thermal cycle and the associated phase changes cause deviations in micro structural and grain sizes and shapes. These welding changes are a challenge to computational models.

2. EQUILIBRIUM DIAGRAMS FOR SS ALLOY

A substance with two or more constituent metallic atoms and metallic bonds predomination are called alloys. The larger constituent is base metal and all others are alloying elements. Equilibrium or phase diagrams give the phase content of the alloy at certain temperature and alloy composition. An equilibrium condition is reversible and is used in temperature changes during heating and cooling as it happens in a welding process. In the ternary phase diagram, stainless steel alloys are based on the base material ferrite (Fe) and cementite (Fe_3C), with concentration as abscissa and temperature as the ordinate. At any point, the %C can be found, even though

*Corresponding author. Tel.: +919849628282
Email address: s4akella@gmail.com (S.Akella)
https://dx.doi.org/10.24951/sreyasijst.org/2016011005
Double blind peer review under responsibility of Sreyas Publications

there are other alloys in the austenitic steel. It is assumed that the phase changes and micro structural transformation are well related to the other alloy elements such as Cr, Ni, Si, Mg etc. Equilibrium diagrams are classified according to the solubility, total or partial in the liquid or solid state and the associated atomic and microstructure.

2.1. Equations

From Kirkaldy's model, a few stages of transformation are given by Goldak. Micro structural transformation can be estimated for low carbon alloys like austenitic steels. The weld heat will reach point 3 at the solid state or point 4 at the liquid state as in the figure A1. Due to the heat flux reaching the bead, the metal at the Heat Affected Zone (HAZ) and Fusion Zone (FZ), moves up from ambient temperature as shown in the figure A2, through regions, 1, 2, 3 to region 4 where solid to liquid transformation occurs. The numerical analysis is shown in equations (2.1) to (2.7).

Liquidus temperature as a function of carbon content is,

$$T_L = 1530.0 - 80.581C \quad (2.1)$$

$$T_S = 1527.0 - 181.356C \quad (2.2)$$

where C is the carbon content in the steel, T_L is the liquidus temperature in ℃ and T_S refers to the solidus temperature.

The austenite grains are pinned by carbide / nitride precipitates which retard the grain growth. The precipitate dissolution temperature at region 4 in the cooling stage after the weld torch has passed the bead and the temperature has retarded, where the grain structure formation is when carbides and nitrides are pinned to the austenite grain at temperature T_S. This can be related as in equation (2.3).

$$T_S = B/(A - \mathrm{Log}[C_m^a C_c^b]) \quad (2.3)$$

where, A=3.11 and B=7520.0 are the constants that dependent on the precipitate species. Concentration of metals Nb, Ti, V is C_m and for nonmetals like nitride, carbide or boride, it is C_c. The stoichiometry constants, a =1.0, and b =1.0 for VC. The upper critical temperature is reached as the temperature cools and metal temperature lowers from region 4 to region 5.

$$A_3(℃) = 912 - 200\mathrm{Sqrt(C)} - 15.2\,\mathrm{Ni} + 44.7\,\mathrm{Si} + 315\,\mathrm{Mo} + 13.1\mathrm{W} - (30\mathrm{Mn} + 11\mathrm{Cr} + 20\,\mathrm{Cu} - 700\mathrm{P} - 400\mathrm{Al} - 120\,\mathrm{As} - 400\mathrm{Ti}) \quad (2.4)$$

where, the compositions are in weight percentages.

The lower critical temperature A_1 for the low alloyed hypo eutectoid steel is given as,

$$A_1(℃) = 723 - 10.7\mathrm{Mn} - 16.9\mathrm{Ni} + 29\mathrm{Si} + 16.9\mathrm{Cr} + 290\mathrm{As} + 6.4\mathrm{W} \quad (2.5)$$

As the temperature cools, the bainite start temperature BS is reached in the region 6, which is indicated that ferrite and pearlite formation is stopped and bainite formation starts at that temperature.

$$BS(℃) = 656 - 58\mathrm{C} - 35\mathrm{Mn} - 75\mathrm{Si} - 15\mathrm{Ni} - 34\mathrm{Cr} - - - - - - - - 41\mathrm{Mo} \quad (2.6)$$

When rapid cooling is done to the heat effected zone, austenite decomposes to martensite below the martensite start temperature MS. This is shown as region 7 in the figure A2.

$$MS(℃) = 561 - 474\mathrm{C} - 35\mathrm{Mn} - 17\mathrm{Ni} - 17\mathrm{Cr} - 21\mathrm{Mo} \quad (2.7)$$

In region 8, the final grain formation is completed as the metal cools down to the ambient temperature. Thus the eight regions of process change explained by earlier authors include the alloy elements in obtaining the equilibrium diagram.

3. CALCULATIONS RESULTS AND DISCUSSION

Table 1 gives the basic elements of SS steel, where the carbon percentage determines the type of SS steel selected. In this study, the equations developed by earlier authors were first evaluated for different regions to obtain the temperature distribution and then verified the consistency of progress in heating up to liquidus temperature and cooling back to the ambient temperature. The process of heating and cooling is a variable that can change because of the welding process such as TIG, EBW, LASER etc., which determines the rate of heat inflow and thus the rate of temperature rise. Similarly, during cooling, normalizing, and annealing process, air water or water quenching determines the formation of the type of steel. A slow annealing cooling in a furnace retains austenite whereas a faster cooling in oil or normalizing results in formation of bainite

and a faster cooling by forced water can lead to martensite formation.

In the weld process, as illustrated in figure A1 (a), the heat that directly meats the base material is the fusion zone and the immediate neighboring area is weld affected zone. These two areas can undergo phase transformation. Figure A1 (b), gives the iron-iron carbide diagram. This diagram will get modified as the alloy elements get added. The regions of phase changes are shown for the regular iron – iron carbide diagram as in figure A1(c). For the hypo eutectoid metal, the welding area is initially at ambient temperature. As heat is added to fusion zone and heat affected zone, the material moves to region 1, which is a combination of ferrite, bainite and martensite. Further heating will move the material to region 2 which is the lower critical temperature A1, 788 ℃, where, austenite formation takes place. This phase change happens till the region reaches the upper critical temperature, A3, which is at 1028 ℃ when it moves to the region 3.

Table 1.Composition of Austenitic SS by %Wt

Chromium	16 – 25
Nickel	1 8 – 20
Manganese	1 – 2
Silicon	0.5 – 3
Carbon (Less than .04 designated as L grade)	0.02-0.08
Molybdenum	0 – 2
Nitrogen	0 - 0.15
Titanium & Niobium	0 - 0.2

In this region, TS temperature is reached where the carbides and nitrides (C_c) of metals (C_m) like V, Nb and Ti pin to the grain boundaries thus, retarding further grain growth and phase transformation. The next region 4 starts when the metal attains the solidus state T_S and ends at the liquidus state T_P or T_L. From here on, the next transformation happens during cooling in region 4 which ends at A3 and enters the region 4 which ends at A1. Next region 5 starts where austenite formed moves to region 6 up to the BS state of bainite or to the region 7 where martensite is formed at MS from where it cools to the ambient temperature in region 8. The temperature phase regions for SS Alloy are also shown.

The addition of elements moves the phase transformation temperatures of the iron – iron carbide equilibrium diagram. A sample calculation was conducted on an SS steel with alloy elements compositions of C=0.05, Cr = 22, Ni=1, Mo=1, Si=0.5, Ti=0.1. This alloy was estimated for different temperatures as given by Goldak.

First, from ambient temperature, martensite phase (MS) was calculated as 125.3 ℃ using equation (2.7). Next the bainite temperature was calculated as 207.4 ℃. To obtain this temperature above MS, the coefficient of Cr was modified from -34 to -13 and modified equation (2.6) was used. In order to obtain the lower austenite critical temperature of A_1, calculation was done and to get a reasonable temperature above BS, the coefficient of Ni was adjusted from -16.9 to -321.1. Here, the modified equation (2.5) was used. The temperature obtained was 788.84 ℃.

The upper critical temperature (A_3) was calculated by modifying equation 4. The coefficient of Ni was changed from -15.2 to -288.8 and for Mo the coefficient changed from 315 to 630. With these changes, the temperature obtained was 1028.8 ℃. Next, the precipitate dissolution temperature (Ts) was calculated. Here, the values given along with equation (2.3) were used as it is and obtained a temperature of 1389.75℃. Above this temperature, the metal will go into solidus phase.

The results of equation (2.2 and 2.1) are used to obtain the solidus (T_S) and liquidus (T_L) temperature. The difference in temperature between these two phases was very small and is within ten degrees. The liquidus and solidus temperature result in a difference of only 10 degrees when the carbon percentage varies from 0.02 to 0.08. For our case, when c is 0.05, the difference is 8.1℃. The results are shown in table 2.

Table 2.Liquidus & Solidus Temp

C	TL	Ts
0.02	1528.4	1523.4
0.03	1527.6	1521.6
0.04	1526.8	1519.7
0.05	1526.0	1517.9
0.06	1525.2	1516.1
0.07	1524.4	1514.3
0.08	1523.6	1512.5

Calculations were done for alloy SS with the given composition. The equations established cannot be generalized. Experimental results are to be used to validate the equations formed. Also these equations are to be used in FEA of welding simulation.

4. CONCLUSION

Phase transformation temperatures were resulted from modified equations from earlier researchers. These equations will be established and used in finite element analysis.

REFERENCES

[1] P.M.Dasami, K.Parameswari, S.Chitra, and K.Jayamoorthy, Experimental and Quantum Chemical Studies on the Corrosion Inhibition of Mild Steel by Quinoline Schiff Bases, DJ Journal of Engineering Chemistry and Fuel, Vol. 1, No. 4, 2016, pp. 1-16, http://dx.doi.org/10.18831/djchem.org/2016041001.

[2] L.Borjesson and L.E.Lindgren, Thermal, Metallurgical & Mechanical Models for Simulation of Multipass Welding, ASME Journal of Engineering Materials and Technology, Vol. 123, 2001, pp. 106-111.

[3] C.H.Muralimohan, S.Haribabu, Y.Hariprasada Reddy, V.Muthupandi and K.Sivaprasad, Joining of AISI 1040 Steel to 6082-T6 Aluminium Alloy by Friction Welding, Journal of Advances in Mechanical Engineering and Science, Vol. 1, No. 1, 2015, pp. 57-64, http://dx.doi.org/10.18831/james.in/2015011006.

[4] J.S.Kirkaldy and D.Venugopalan, Prediction of Microstructure and Hardenability in Low Alloy Steels. International Conference on Phase Transformations in Ferrous Alloys, TMS-AIME, Warrendale, 1983, pp. 125-148.

[5] M.Ganesan, S.Johny James and P.Santhamoorthy, Design to Replace Steel Drive Shaft in Automobiles with Hybrid Aluminium Metal Matrix Composite Journal of Advances in Mechanical Engineering and Science, Vol. 1, No. 3, 2015, pp. 41-48, http://dx.doi.org/10.18831/james.in/2015031005.

[6] John A.Goldak and Mehadi Akhloghi, Computational Welding Mechanics, Springer Science and Business Media, New York, 2006.

[7] G.Venses and R.Sri Siva, Optimisation of Deep Cryogenic Treatment Process on the Wear Resistance of 100Cr6 Bearing Steel using Taguchi Technique, Journal of Advances in Mechanical Engineering and Science, Vol. 1, No. 2, 2015, pp. 9-20, http://dx.doi.org/10.18831/james.in/2015021002 2455-0957.

[8] L.E.Lindgren, Computational Welding Mechanics: Thermomechanical and Microstructural Simulations, Woodhead Publishing, England, 2007.

APPENDIX

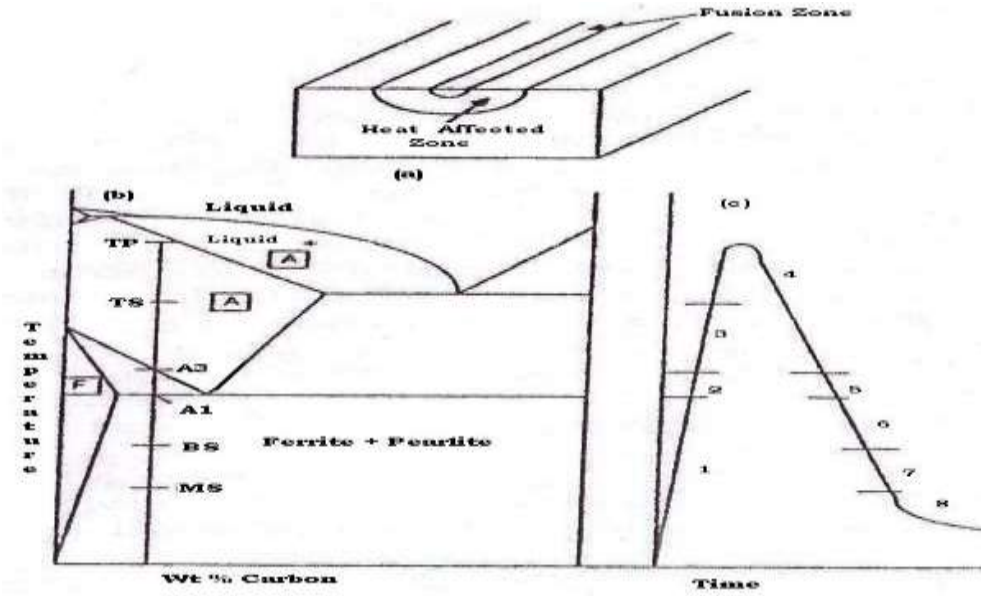

Figure A1.Equilibrium diagram

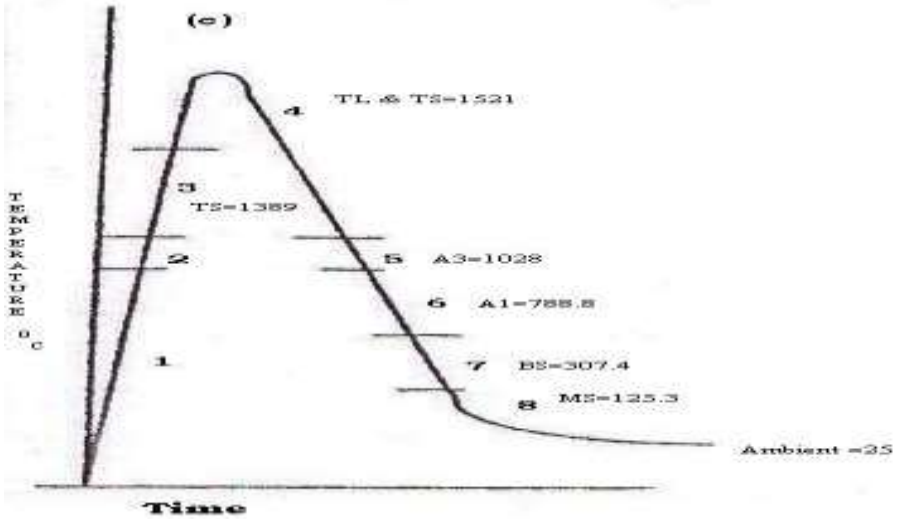

Figure A2.Hypoeutectoid SS alloy phases